Improvement of usability of power-assisted cart with torque sensor built in driving wheel

Ryohei Kitayoshi*a) Member, Hiroshi Fujimoto** Senior Member

Recently, a lot of handcarts, power-assisted carts and autonomous mobile robots have been used in the field of production and welfare. Accordingly usability of these devices for users has become more important than ever before. In this paper, we show that usability of power-assisted cart driven by servo motors is improved by controlling precisely acceleration of car body with torque sensor incorporated in driving wheel and force sensor attached on the control lever.

Keywords: Power-assisted cart, Usability, Torque sensor, Impedance control, Acceleration control

1. Background

Recently, a lot of handcarts, power-assisted carts and autonomous wheel robots have been used in the field of production and welfare. For example, the handcart put on a cooperative robot shown in Fig.1 [(1)] is released by Yaskawa Electric Corporation. Accordingly usability of the devices for users has become more important than ever before. For improvement of usability, downsizing and lightening of actuators are needed and small-sized flat reduction gears are often used. However, the reduction gear has some faults : low rigidity, back lash, lost motion and so on. These faults prevent from precise power-assist control and cause a loss of usability.

For solving this problem, many researches have been conducted in recent years. Previous studies [(2) (3)] indicate that controlling accurately output torque of reduction gear by load-side encoder and torque sensor. Akada et al. [(4)] demonstrated control of power-assisted cart with wheel-side encoder. Kuroki et al. [(5)] developed a noble torque sensor for precise measurement of joint torque and control of human support robot. Research on estimation of output torque [(6) (7)] has been performed. However, there has been no study on control acceleration of power-assisted cart by joint torque feedback measured by torque sensor.

In this paper, we show that usability of power-assisted cart driven by harmonic reduction gear is improved by controlling acceleration of wheel with torque sensor built in driving wheel. In section 2, we explain an overview of mechanism of the power-assisted cart and construct dynamic model needed for controller design and simulation. In section 3, we propose two acceleration control methods. In section 4, we define two evaluation values for estimation of proposal control method. In section 5 and 6, we demonstrate validity of the proposal control method by simulation and experiment.

Fig. 1. Example of handcart in the field of production

2. Power-assisted Cart

In this section, we explain an overview of mechanism of power-assisted cart and construct dynamic model needed for design of control system and simulation.

2.1 Overview of mechanism Power-assisted cart consists of three parts : Actuator, Control lever and Load in Fig.2. The cart is driven by the two actuators and one passive wheel. The passive wheel has an encoder for measuring velocity and acceleration of the cart. The actuator in Fig.3 has driving parts and measuring devices. The driving parts are a servo motor (Yaskawa Electric Corporation product Type:SGMMV-A2A2A) and a harmonic reduction gear (Harmonic Drive Systems product Type:CSF-14-30-2UH). The servo motor and reduction gear drive a wheel.

The measuring devices are a torque sensor and a load side encoder. The torque sensor is built in driving wheel and capable of measuring precisely torque generated by the reduction gear. The load side encoder measures rotation angle of the wheel.

The control lever has a force sensor. The force sensor mea-

a) Correspondence to: Ryohei.Kitayoshi@yaskawa.co.jp
* Corporate Research & Development Center YASKAWA ELECTRIC CORPORATION, 12-1 Otemachi, Kokurakita-ku, Kitakyushu 803-8530 Japan

** University of Tokyo, 5-1-5 Kashiwanoha, Kashiwa, Chiba, 277-8561, Japan

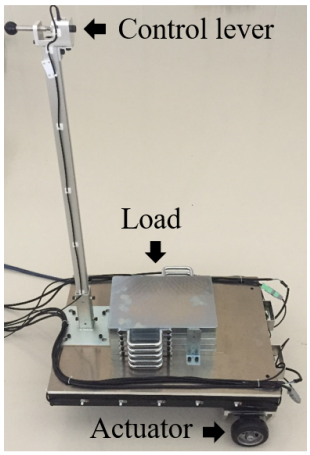

Fig. 2. Overview of power-assisted cart

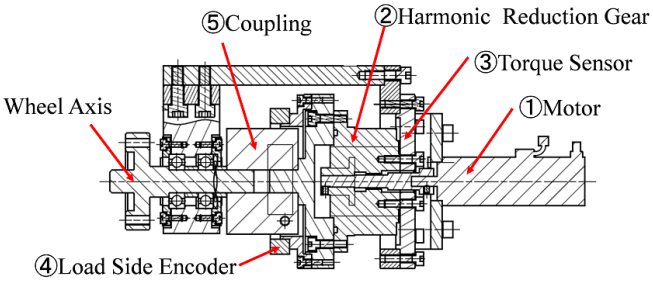

Fig. 3. Structure of actuator

sures operating force which is applied to the cart when the user pushes or pulls the cart. The load is used for changing mass of the cart. Mass of the cart is changed from 40 kg to 80 kg per 10 kg by adjusting the number of load.

2.2 Strict dynamic model Dynamic model of the cart consists of two-mass system and nonlinear system in Fig.4 and Table.1. This model is called as "strict dynamic model" hereafter. The two-mass system expresses dynamic behavior of driving parts in the actuator. The motor and wheel are expressed as a rigid body and the reduction gear is expressed as elastic element because stiffness of the reduction gear is lower than other driving parts.

The nonlinear system expresses that the cart is driven by driving force which is nonlinear friction between the wheel and ground. The driving force F_d is determined by road friction coefficient μ and vertical force F_v shown in Eq.(1). Road friction coefficient is determined by magic formula which is nonlinear relation between road friction coefficient and slip ratio λ shown in Eq.(2), (3). This nonlinear relation is shown in Fig.5. Red zone of Fig.5 is called cohesive zone where the nonlinear relation is considered to be linear.

$$F_d = \mu F_v \quad \cdots\cdots (1)$$

$$\mu = D \cdot \sin\left(C \cdot \tan^{-1}\phi\right) \quad \cdots\cdots (2)$$

$$\phi = B \cdot \left[(1-E)\cdot\lambda + \frac{E}{B}\cdot\tan^{-1}(B\cdot\lambda)\right] \quad \cdots\cdots (3)$$

$$B = 26.66 \quad C = 1.40 \quad D = 0.18 \quad E = 0.40$$

2.3 Approximate dynamic model The nonlinear system makes difficult to design controller and so we construct dynamic model with only linear two-mass system shown in Fig.6 by assuming that the cart moves in cohesive zone. This model is called as "approximate dynamic model" hereafter. Based on the assumption, mass of cart M is considered to be part of wheel-side inertia and total of wheel-side inertia J_{all} is expressed in Eq.(4) on previous research [8]. In next section, we design acceleration controller based on the approximate dynamic model.

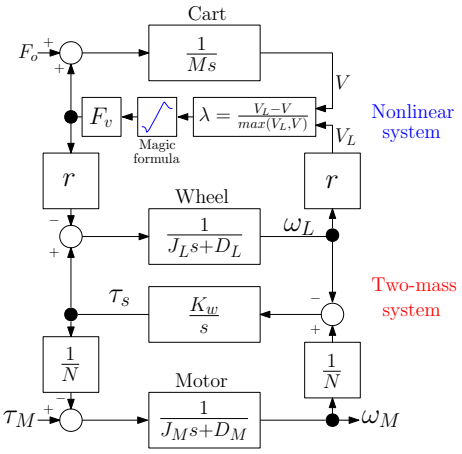

Fig. 4. Block diagram of strict dynamic model

Table 1. A list of symbols in strict dynamic model

Symbol	Name	Unit
M	Mass of Cart	kg
J_M	Motor Inertia	kgm^2
J_L	Wheel Inertia	kgm^2
r	Radius of Wheel	m
ω_M	Motor-side Angular Velocity	rad/s
ω_L	Wheel-side Angular Velocity	rad/s
τ_M	Motor Torque	Nm
τ_s	Joint Torque	Nm
V	Car body Velocity	m/s
V_L	Wheel Velocity	m/s
F_d	Driving force	N
F_o	Operating force	N
K_w	Stiffness of Reduction Gear	Nm/rad
μ	Road Friction Coefficient	-
λ	Slip Ratio	-
N	Ratio of Reduction Gear	-

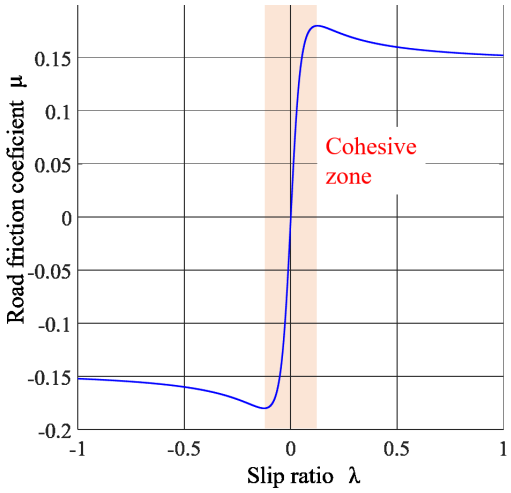

Fig. 5. Magic formula

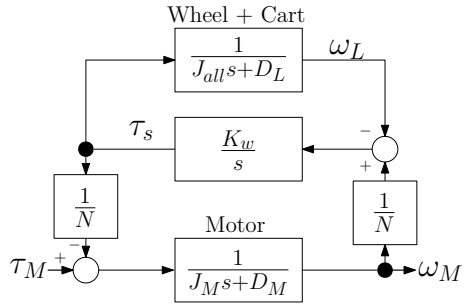

Fig. 6. Block diagram of approximate dynamic model

Table 2. Parameters of approximate dynamic model

Symbol	Name	Number	Unit
J_m	Motor Inertia	4.0×10^{-6}	kgm^2
J_{all}	Total Inertia	1.8×10^{-1}	kgm^2
D_M	Motor Viscous Coefficient	4.3×10^{-5}	Nms/rad
D_L	Wheel Viscous Coefficient	1.1×10^{-1}	Nms/rad
K_w	Stiffness of Reduction Gear	1.9×10^{3}	Nm/rad
M	Mass of Cart	80.6	kg
r	Radius of Wheel	0.05	m
N	Reduction Ratio	31	-
λ	Slip Ratio	0.1	-

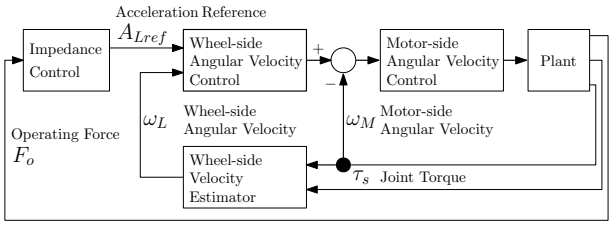

Fig. 7. Block diagram of Control system

$$J_{all} = J_L + Mr^2(1-\lambda) \cdots\cdots (4)$$

3. Control system

In this section, we propose a control system for controlling the acceleration of the power-assisted cart . The control system shown in Fig.7 is composed of three parts : Impedance controller, acceleration controller and wheel-side velocity estimator. The impedance controller generates acceleration reference according to operating force. The acceleration controller calculates torque reference to the servo drive based on the acceleration reference, wheel-side angular velocity and motor-side angular velocity. The wheel-side velocity estimator calculates wheel-side velocity from joint torque measured by torque sensor and motor-side angular velocity measured by motor encoder.

3.1 Impedance control The Impedance control generates wheel-side angular acceleration reference A_{Lref} from operating force F_o in Eq.(5). M_v expresses a virtual mass. The virtual mass is configured as 40.3 kg and this value is half of the cart.(Mass of the cart is 80.6 kg).

$$A_{Lref} = \frac{F_o}{M_v r} \cdots\cdots (5)$$

3.2 Acceleration controller The acceleration control is composed of two part : wheel-side velocity controller and motor-side velocity controller. We propose two ways of controller design corresponding to target performance. The target performance is high accuracy and high command response of acceleration.For high accuracy, both of controllers are I-P controller in order to converge wheel-side velocity and motor-side velocity to reference without deviation. This controller is called as IP-IP controller.For high command response, wheel-side velocity controller is PI controller and motor-side velocity is P controller in order to converge to reference as fast as possible. This controller is called as PI-P controller.

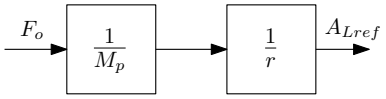

Fig. 8. Block diagram of Impedance control

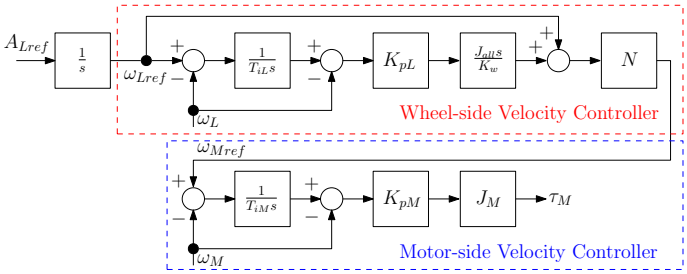

Fig. 9. Block diagram of IP-IP controller

Table 3. Parameters of IP-IP controller

Symbol	Name	Value
ω_p	Pole of transfer function	$55 \times 2\pi$
K_{pM}	Proportional gain of motor-side velocity controller	1.38×10^3
T_{iM}	Integral time of motor-side velocity controller	3.70×10^{-3}
K_{pL}	Proportional gain of wheel-side velocity controller	6.52×10^2
T_{iL}	Integral time of wheel-side velocity controller	1.45×10^{-2}

3.2.1 IP-IP controller IP-IP controller is shown in Fig.9. Transfer function from acceleration reference A_{Lref} to acceleration A_L is illustrated in Eq.(6) ~ (10). The parameter of controller in Table.3 is designed by pole placement method and coefficient comparison. Poles of the transfer function ω_p are fourfold root shown in Eq.(11). And then making comparison between coefficients of Eq.(6) and coefficients of Eq.(11) constructs four simultaneous equations shown in Eq.(12)

$$\frac{A_L}{A_{Lref}} = \frac{a_0}{s^4 + a_3 s^3 + a_2 s^2 + a_1 s + a_0} \cdots\cdots (6)$$

$$a_0 = \frac{K_{pM}K_{pL}}{T_{iM}T_{iL}} \cdots\cdots (7)$$

$$a_1 = \frac{K_{pM}K_{pL}}{T_{iM}} + \frac{K_{pM}D_L}{T_{iM}J_{all}} + K_{pM}\frac{K_wJ_{all}}{+}\frac{D_LK_w}{J_mJ_{all}N^2} + \frac{D_mK_w}{J_mJ_{all}} \cdots\cdots (8)$$

$$a_2 = \frac{K_{pM}}{T_{im}} + K_{pM}\frac{D_L}{J_{all}} + K_w\left(\frac{1}{J_{all}} + \frac{1}{J_mN^2}\right) + \frac{D_MD_L}{J_MJ_{all}} \cdots\cdots (9)$$

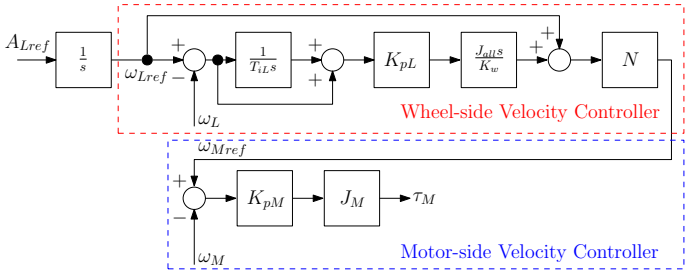

Fig. 10. Block diagram of PI controller

Table 4. Parameters of PI-P controller

Symbol	Name	Value
ω_p	Pole of transfer function	$70 \times 2\pi$
K_{pM}	Proportional gain of motor-side velocity controller	1.31×10^3
T_{iM}	Integral time of motor-side velocity controller	-
K_{pL}	Proportional gain of wheel-side velocity controller	3.70×10^2
T_{iL}	Integral time of wheel-side velocity controller	3.04×10^{-5}

$$a_3 = K_{pM} + \frac{D_M}{J_M} + \frac{D_L}{J_L} \cdots\cdots (10)$$

$$\frac{A_L}{A_{Lref}} = \frac{\omega_p^4}{s^4 + 4\omega_p s^3 + 6\omega_p^2 s^2 + 4\omega_p^3 s + \omega_p^4} \cdots\cdots (11)$$

$$\begin{cases} a_0 = \omega_p^4 \\ a_1 = 4\omega_p^3 \\ a_2 = 6\omega_p^2 \\ a_3 = 4\omega_p \end{cases} \cdots\cdots (12)$$

3.2.2 PI-P controller PI-P controller is shown in Fig.10. Transfer function from acceleration reference A_{Lref} to acceleration A_L is illustrated in Eq.(13) ~ (16). The parameter of controller in Table.4 is designed by pole placement method and coefficient comparison. Poles of the transfer function ω_p are triple root shown in Eq.(17). And then making comparison between coefficients of Eq.(13) and coefficients of Eq.(17) constructs four simultaneous equations shown in Eq.(18).

$$\frac{A_L}{A_{Lref}} = \frac{b_0}{s^3 + b_2 s^2 + b_1 s + b_0} \cdots\cdots (13)$$

$$b_0 = \frac{D_M K_w}{J_M J_{all} N^2} + \frac{K_{pM} K_{pL}}{T_{iL}} + \frac{K_w K_{pM}}{J_{all}} + \frac{D_M K_w}{J_M J_{all}} \cdots\cdots (14)$$

$$b_1 = \frac{K_w K_{pM}}{J_{all}} + K_{pM} K_{pL} + K_w\left(\frac{1}{J_{all}} + \frac{1}{J_M N^2}\right) + \frac{D_M D_L}{J_M J_{all}} \cdots\cdots (15)$$

$$b_2 = K_{pm} - \frac{D_M}{J_M} - \frac{D_L}{J_{all}} \cdots\cdots (16)$$

$$\frac{A_L}{A_{Lref}} = \frac{\omega_p^3}{s^3 + 3\omega_p s^3 + 3\omega_p^2 s + \omega_p^3} \cdots\cdots (17)$$

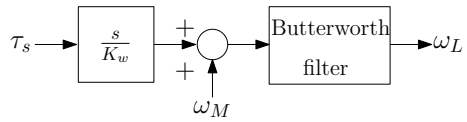

Fig. 11. Block diagram of wheel-side velocity estimator

$$\begin{cases} b_0 = \omega_p^3 \\ b_1 = 3\omega_p^2 \\ b_2 = 3\omega_p \end{cases} \cdots\cdots (18)$$

3.3 Wheel-side velocity estimator Wheel-side velocity estimator is shown in fig.11. Wheel-side velocity ω_L is calculated from motor-side velocity ω_M and joint torque τ_s by Eq.(19). Joint torque is measured by the torque sensor and 4th order butterworth filter is used for elimination of noise in a high frequency of the torque sensor. Cut-off frequency of the butterworth filter is configured as 300 Hz.

$$\omega_L = \omega_M + \frac{\tau_s s}{K_w} \cdots\cdots (19)$$

4. Evaluation values

In this section, we introduce two evaluation values :"Sensation mass "M_s and "Response time" T_r for estimating proposal control method. "Sensation mass" M_s is weight which user feels when moving the power-assisted cart and is calculated by Eq.(20), (21). "Response time" T_r is a period after motor starts to move until sensation mass reaches the virtual mass. Time when motor starts to move is defined as time when motor-side velocity is over 100[rpm]. Time when sensation mass reaches the virtual mass is defined as time when sensation mass enters between virtual mass $M_v \pm 5\%$.

$$F_o = M_s A_c \cdots\cdots (20)$$

$$M_s = \frac{F_o}{A_c} \cdots\cdots (21)$$

5. Simulation

In this section, we show effect of proposal controllers based on the evaluation values by simulation. In simulator an user applies constant force to the cart and sensation mass and response time is evaluated during operation.

5.1 Condition In simulation, strict dynamic model is used as model of plant. Reference of operating force is step-like signal filtered by low-pass filter of which cut-off frequency is 10 Hz and amplitude of the reference is 8 m/s^2(converted acceleration value). The low pass filter is assumed to be frequency response characteristic of human. For comparison with our proposal method, we perform simulation in the case of acceleration control with only motor-side velocity controller shown in Fig.12 and 15. The parameter of controller is used in Table.3 and 4.

5.2 Result As illustrated in Table.5, the deviation of sensation mass of IP-IP controller is the least and the response time of PI-P controller is shortest in all of the method.

Table 5. Simulation result

Type of controller	IP-IP	IP	PI-P	P
Error of sensation mass M_s [%]	1.69	1.72	1.84	2.47
Response time T_r [s]	0.110	0.124	0.019	0.438

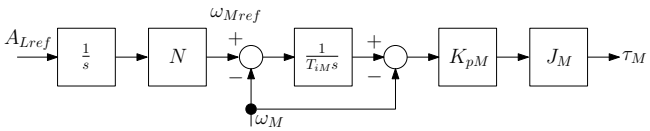

Fig. 12. Block diagram of motor-side velocity IP control

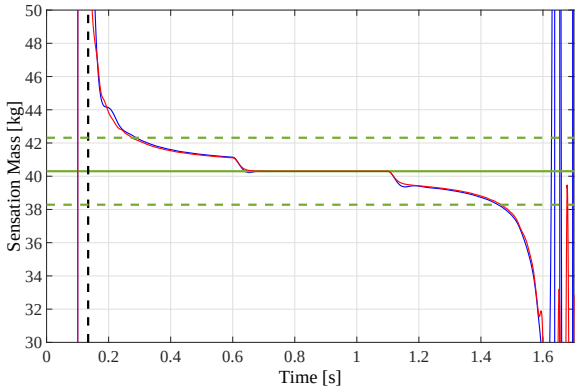

Fig. 13. Time response of Sensation Mass in case fo IP-IP control

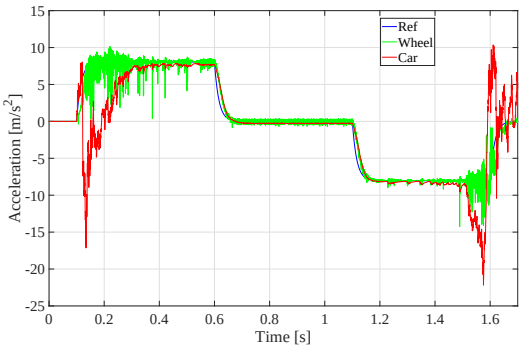

Fig. 14. Time response of acceleration in case of IP-IP control

5.2.1 IP-IP controller Sensation mass follows accurately to virtual mass shown in Fig.13. Red line is time response of sensation mass in case of IP-IP controller. Blue line is time response of sensation mass in case of IP controller. Green line is value of virtual mass M_v : 40.3 kg. Green dashed line is $M_v \pm 5\%$. Black dashed line is start of movement. We define the start as time when motor-side velocity is over 100 rpm and the end as time when motor-side velocity is under 100 rpm. Acceleration of wheel also follows accurately to the reference in Fig.14. Deviation between acceleration of wheel and cart is generated by slip when accelerated and decelerated.

5.2.2 PI-P controller Sensation mass follows fast to virtual mass in Fig.16. Red line is time response of sensation mass in case of PI-P controller. Blue line is time response of sensation mass in case of P controller. Green line is value of virtual mass M_v : 40.3 kg. Green dashed line is

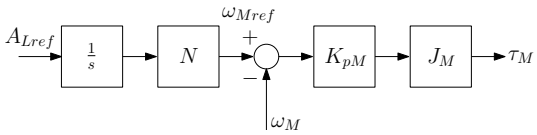

Fig. 15. Block diagram of motor-side velocity P control

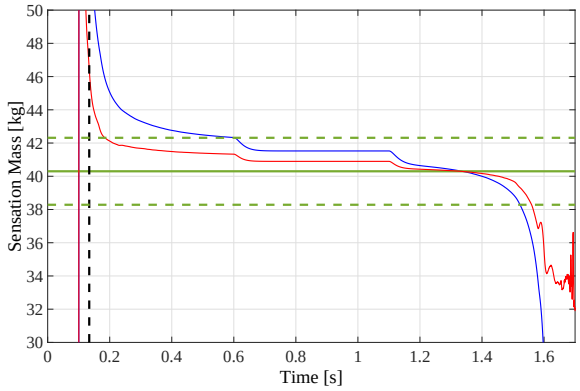

Fig. 16. Time response of Sensation Mass in case of PI-P control

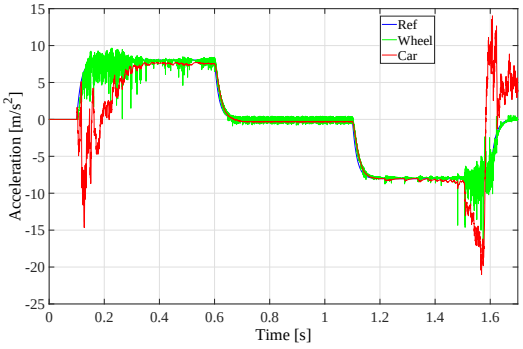

Fig. 17. Time response of acceleration in case of PI-P control

$M_v \pm 5\%$. Black dashed line is start of movement. Acceleration of wheel also follows fast to the reference in Fig.17. Deviation between wheel acceleration and car acceleration is generated by slip when accelerated and decelerated.

6. Experiment

We demonstrate effectiveness of proposal controller by converging sensation mass to virtual mass precisely and fast by experiment.

6.1 Condition While controlling acceleration by our proposal controller, the power-assisted cart is moved back and forward straight for 2 m by pushing or pulling control lever with hand (shown in Fig.18). The virtual mass is configured as 40.3 kg and is half of mass of the cart. For comparison with our proposal method, we made experiments in the case of acceleration control with only motor-side velocity controller shown in Fig.12 and 15. The parameter of controller is used in Table.3 and 4.

6.2 Result As illustrated in Table.6, the deviation of sensation mass of IP-IP controller is the least and the response time of PI-P controller is shortest in all of the method. Time response of sensation mass is shown in Fig.19 and 20.

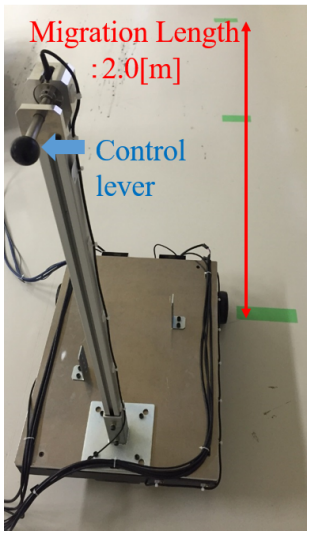

Fig. 18. Situation of experiment condition

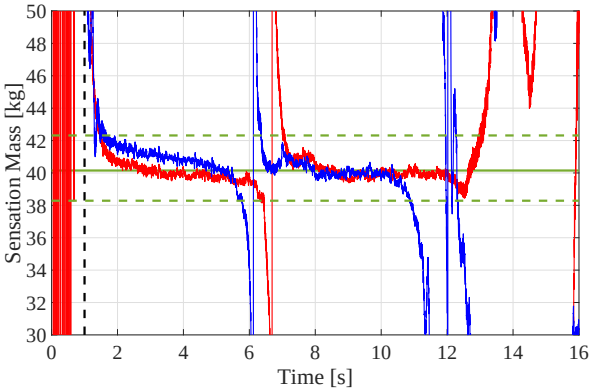

Fig. 19. Comparison of time response of sensation mass in case of IP-IP control

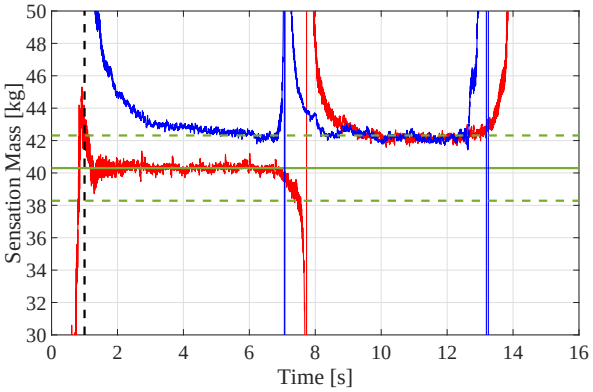

Fig. 20. Comparison of time response of sensation mass in case of PI-P control

In the figure, blue line is time response of sensation mass in case of proposal control, green line is time response of sensation mass in case of only motor-side velocity control and red line is virtual mass. In Fig.19, the green line converges to the red line with less deviation from 2 to 5 s and from 8 to 11 s.In Fig.20, the green line reach an area between red dashed lines faster from 1 to 2 s.

Table 6. Experimental result

Type of controller	IP-IP	IP	PI-P	P
Error of sensation mass M_s [%]	1.23	1.50	2.36	3.30
Response time T_r [s]	0.505	0.665	0.128	5.150

7. Conclusion

In this paper, we show that usability of power-assisted cart driven by servo motors is improved by controlling precisely acceleration of car body with torque sensor built in driving wheel. The acceleration controller realizes the high command response and a steady state with less deviation enough that sensation mass converges to virtual mass.

However, there are two future problems. One is deviation between virtual mass and sensation mass because of wheel slip. Wheel slip disturbs precise acceleration control and cause the deviation. We think that wheel slip can be suppressed by adding velocity limiter to the velocity controller. The other is an incorrect action because of offset error of force sensor. The offset error generates unnecessary acceleration reference and causes the incorrect action. We tried adding a high pass filter to the impedance controller in order to eliminate the offset error. But the high pass filter deteriorates the operability because it eliminates not only offset error but also low frequency band component of operating force. As a result, we think that a physical switch is needed at the control lever in order to detect whether users contact with the cart or not.

We will develop more practical and useful control method while considering the problems.

References

(1) Yaskawa Electric Corporation News Release : https://www.yaskawa.co.jp/newsrelease/product/56674 (Last browsed time : 2018/12/1)

(2) S. Yamada, K. Inukai, H. Fujimoto, K. Omata, Y. Takeda, S. Makinouchi, ”Joint torque control for two-inertia system with encoders on drive and load sides”, IEEE 13th International Conference on Industrial Informatics, Cambridge United Kingdom, pp. 396 – 401, 2015

(3) Y. Kawai, Y. Yokokura, K. Ohishi, ”High Back-drivable Pseudo I-PD Torque Control Using Load-side Torque Observer With Torsion Torque Sensor”, IEEE 14th International Workshop on Advanced Motion Control, Auckland New Zealand, pp. 175–180, 2016

(4) W. Akada, H. Fujimoto : ” Study on Power Assist Control of Push Cart Robot with Wheel-Side Encoder ”, IEEJ International Workshop on Sensing, Actuation, Motion Control, and Optimization, 2016.

(5) Y. Kuroki, Y. Kosaka, T. Takahashi, E. Niwa, H. Kaminaga, and Y. Nakamura: “Cr–N Alloy Thin–film Based Torque Sensors and Joint Torque Servo Systems for Compliant Robot Control”, Proc. IEEE International Conference on Robotics and Automation (ICRA), pp. 4954–4959, May. 2013.

(6) J. Lee, C. Lee, N. Tsagarakis, and S. Oh: “Residual Based External Torque Estimation in Series Elastic Actuators Over a Wide Stiffness Range: Frequency Domain Approach”, IEEE Robotics and Automation Letters, vol. 3 no. 3, pp. 1442–1449, Jul. 2018.

(7) Y. Yamada and Y. Kakinuma: “Sensorless cutting force estimation for full-close controlled ball-screw-driven stage”, The Int. J. Advanced Manufacturing Technology, vol. 87, no. 9, pp. 3337–3348, Dec. 2016

(8) K. Fujii, H. Fujimoto, : ”Traction Control based on Slip Ratio Estimation Without Detecting Vehicle Speed for Electric Vehicle” Power Conversion Conference, Nagoya, April. 2007.

(9) H.B.Pacejka, and E.Bakker, “The Magic Formula Tyre Model”, Proc. 1st International Colloquium on Tyre Models for Vehicle Dynamics Analysis, held in Delft, The Netherlands, Oct 21-22 (1991)